The Seasonal Effects of ENSO on European Precipitation: Observational Analysis

JEFFREY SHAMAN

Department of Environmental Health Sciences, Columbia University, New York, New York

(Manuscript received 26 December 2013, in final form 29 May 2014)

ABSTRACT

An analysis and characterization of seasonal changes in the atmospheric teleconnection between ENSO and western European precipitation, as well as atmospheric conditions over the North Atlantic and Europe, are presented. Significant ENSO-associated changes in precipitation are evident during the boreal spring and fall seasons, marginal during boreal summer, and absent during boreal winter. The spring and fall precipitation anomalies are accompanied by statistically significant ENSO-related changes in large-scale fields over the North Atlantic and Europe. These seasonal teleconnections appear to be mediated by changes in upper tropospheric conditions along the coast of Europe that project down to the lower troposphere and produce onshore or offshore moisture flux anomalies, depending on the season. Some ENSO-related changes in storm activity are also evident during fall and winter. Analyses during boreal winter reveal little effect of coincident ENSO conditions on either European precipitation or upper tropospheric conditions over Europe.

1. Introduction

A considerable body of literature exists documenting the seasonal covariability between El Niño–Southern Oscillation (ENSO) and weather conditions over Europe. Observational studies indicate an association present during boreal winter between ENSO variability and European surface meteorological conditions, including temperature, precipitation, and sea level pressure (van Loon and Madden 1981; Fraedrich 1994; Pozo-Vázquez et al. 2001; Moron and Gouirand 2003; Moron and Plaut 2003; Zanchettin et al. 2008; Ineson and Scaife 2009), river flow (Niedzielski 2011), and upper tropospheric conditions (Dong et al. 2000). Other studies have provided evidence for various teleconnections between regional European conditions and ENSO during boreal spring (Rodó et al. 1997), summer (Park 2004), and autumn (Rodó et al. 1997; Mariotti et al. 2002; Park 2004; Vicente-Serrano 2005; Shaman and Tziperman 2011).

Precipitation variability in association with ENSO is the focus of this work, and this association with ENSO varies both seasonally and regionally within Europe. During summer and fall increased precipitation over southern Europe occurs when El Niño conditions prevail in the equatorial Pacific (Mariotti et al. 2002; Park 2004), whereas negative anomalies develop over the region during spring (Shaman and Tziperman 2011). Over Scandinavia, negative wintertime precipitation anomalies have been shown to develop during coincident El Niño events (Fraedrich 1994). More recent studies have found increased wintertime precipitation over Britain, France, and Germany during an El Niño, but decreased precipitation over Scandinavia (Zanchettin et al. 2008).

A second suite of studies has found lagged associations between Northern Hemisphere wintertime ENSO conditions and precipitation the following spring in a number of regions, including southwestern Europe (Rodó et al. 1997; Knippertz et al. 2003), central Europe (Lloyd-Hughes and Saunders 2002), and Scandinavia (Feddersen 2003). Evidence for lagged correlations between ENSO and precipitation during other seasons has also been observed (Efthymiadis et al. 2007). Some of these lag associations may stem from the seasonal persistence of SST anomalies in the tropical Pacific.

Here, observational analyses of seasonal teleconnections between ENSO and precipitation over the European continent are explored systematically for the entire calendar year. Previous works have examined seasonal ENSO teleconnections with precipitation around the entire planet (Ropelewski and Halpert 1986; Mason and

Corresponding author address: Jeffrey Shaman, Department of Environmental Health Sciences, Mailman School of Public Health, Columbia University, 722 West 168th Street, Rosenfield Building, Room 1104C, New York, NY 10032.
E-mail: jls106@columbia.edu

DOI: 10.1175/JCLI-D-14-00008.1

Goddard 2001); however, in this work the relationship of both ENSO and European precipitation with upper tropospheric variability, the level at which atmospheric ENSO teleconnections mediated by tropospheric Rossby waves are typically evident, is also examined explicitly. The focus is on contemporaneous seasonal teleconnections—that is, teleconnections expected to be mediated through the atmosphere on intraseasonal time scales. As a consequence, lagged associations are not investigated.

This work endeavors to document how the ENSO–European precipitation teleconnection, as manifest during 1950–2013, varies with season. A second article (Shaman 2014) further examines the mechanisms of the atmospheric teleconnection in the upper troposphere using a suite of model experiments. Section 2 of this work presents the data and methods. Section 3 presents observational analysis of precipitation and upper and lower tropospheric conditions. The seasonal relationship between ENSO and the North Atlantic Oscillation (NAO) is presented in section 4. Section 5 presents a maximum covariance analysis of precipitation and upper tropospheric conditions. Section 6 provides discussion.

2. Data and methods

Analyses of precipitation were performed using the European Climate Assessment and Dataset (ECA&D). Specifically, 1950–2013 0.5° regular gridded E-OBS daily precipitation data (version 10.0) were used (Haylock et al. 2008). Additional analyses were performed using three monthly satellite-derived precipitation datasets: 1) the 1979–2011 National Oceanic and Atmospheric Administration (NOAA) National Centers for Environmental Prediction (NCEP) Climate Anomaly Monitoring System (CAMS) Outgoing Longwave Radiation Precipitation Index (OPI) (Janowiak and Xie 1999); 2) the 1979–2008 National Aeronautics and Space Administration (NASA) Global Precipitation Climatology Project (GCPC) version 2.1 (Adler et al. 2003); and 3) the 1979–2010 NOAA NCEP Climate Prediction Center (CPC) Merged Analysis of Precipitation (CMAP) (Xie and Arkin 1997). All three satellite-derived datasets are gridded at 2.5° × 2.5° resolution. The CAMS OPI and NASA GCPC precipitation are both derived from satellite and gauge estimates. The CMAP precipitation is a merging of satellite estimates, gauge estimates, and numerical predictions. The ECA&D data are land only and derived from station observations.

A number of reanalysis fields were included in the analysis. These fields were restricted to the 1950–2013 time period to match the period of the ECA&D precipitation data. In particular, monthly NCEP–NCAR reanalysis (NNR) atmospheric fields (Kalnay et al. 1996), including relative vorticity, temperature, horizontal wind, and specific humidity, were used. In addition, daily NNR data were used to diagnose and analyze changes in storm activity associated with ENSO. 1950–2013 monthly average sea surface temperature for the Niño-3.0 region (5°N–5°S, 150°–90°W) was the index of ENSO used for this study (Kaplan et al. 1998).

European seasonal weather is strongly affected by the NAO (Hurrell and van Loon 1997; Rodó et al. 1997; Rimbu et al. 2001; Efthymiadis et al. 2007). Consequently, the seasonal effects of the NAO on European precipitation, as well as its covariability with ENSO, were also explored. Two indices of the NAO were used in this study: 1) a 1950–2013 monthly principal component (PC)–based index of Hurrell (NCAR 2013), and 2) a 1950–2013 monthly station-based index from the Climate Research Unit (CRU) (Jones et al. 1997). The first NAO index is the time series of the leading empirical orthogonal function of sea level pressure anomalies for 20°–80°N and 90°W°–40°E. Unlike station-based measures, this form of the NAO is not derived from fixed stations but instead flexibly tracks shifts in the centers of action of the NAO. The CRU index is derived from station sea level pressure observations in Gibraltar and Rekyjavik, Iceland.

Both the Niño-3.0 and NAO indices were used for constructing seasonal composites of other fields. Specifically, for a given season (e.g., January–March, April–June, etc.), years for which the chosen index was in excess of plus or minus one standard deviation were identified. For a particular field (e.g., precipitation), seasonal composites were then constructed by subtracting conditions for that same season averaged for all negative phase (e.g., La Niña) years from conditions for that same season averaged for all positive phase (El Niño) years. As an example, positive precipitation anomalies would indicate increased precipitation during an El Niño event and/or decreased precipitation during a La Niña event.

The statistical significance of a given composite was first assessed on a point-by-point basis through the generation of 5000 random composite maps. For instance, for the January–March (JFM) season, there were 7 El Niño and 10 La Niña ±1 standard deviation years during the 1950–2013 period. Consequently, each of the 5000 random composites was generated by averaging 10 randomly selected years from the 1950–2013 JFM record and subtracting this mean field from the average of 7 randomly selected years. The generated distribution of 5000 random composite values was then used to assess statistical significance on a point-by-point basis; that is, a composite point was deemed significant at $p < 0.05$ if it lay below the 2.5th or above the 97.5th percentiles of the generated distribution of composite values for that respective point.

In addition, the whole composite field statistical significance for the North Atlantic/European sector (30°–70°N, 60°W–40°E) was assessed, per the methods of Livezey and Chen (1983). Specifically, 500 additional random composites were generated and each of these was assessed for statistical significance on a point-by-point basis using the same distribution of 5000 random composite values. The number of statistically significant points was then tallied for each of the 500 additional random composites to generate a bootstrapped distribution of field significance. Whole field statistical significance for the observed composite was then assessed as the total number of statistically significant points evaluated against this second bootstrapped distribution.

As the atmospheric response to equatorial forcing occurs on subseasonal time scales (i.e., planetary waves reach the North Atlantic from the Pacific in less than one week), the analysis was limited to simultaneous seasonal comparison of Pacific and European conditions. Seasonal lags were not examined nor were comparisons made to a reference year of ENSO phase (e.g., as in Kiladis and Diaz 1989). Rather, an ENSO event, either El Niño or La Niña, merely reflects deviation in excess of ±1 standard deviation from the seasonal mean.

Maximum covariance analysis (MCA) was also performed to determine if the dominant modes of interannual covariability among two fields would yield spatial loading patterns similar to ENSO or NAO composites of individual fields. This analysis was used to validate the role of the upper troposphere over the North Atlantic and Europe as an intermediary between ENSO and European precipitation. MCA was used to derive pairs of spatial patterns from the cross-covariance matrix of the two fields (Bretherton et al. 1992; Von Storch and Zwiers 2001). Both fields were standardized prior to calculation of the cross-covariance matrix and decomposition.

The leading spatial patterns were then spatially correlated with ENSO or NAO composites of the same fields to determine if the dominant structures representing covariability between European precipitation and upper tropospheric conditions over the North Atlantic and Europe are themselves associated with ENSO or NAO variability. To assess the statistical significance of these spatial correlations, 5000 random seasonal ENSO and NAO composites were again generated and used to bootstrap distributions of spatial correlation.

3. Observational analysis

a. Analyses of precipitation

Seasonal ENSO-based composites of ECA&D precipitation were made using Niño-3.0 SSTs (Fig. 1). During the January–March season there is little ENSO-associated change of precipitation over most of Europe, except for a precipitation decrease during El Niño events that maximizes over southwestern Scandinavia and Scotland, and some positive anomalies between 20° and 30°E over northern Finland, Lithuania, Belarus, and Romania. During April–June (AMJ) more pronounced positive anomalies are evident over France and Britain. Positive anomalies over Scandinavia are also manifest, as has been documented previously (Feddersen 2003).

In boreal summer, July–September (JAS), statistically significant negative precipitation anomalies are centered over northern Europe, including the Netherlands, Germany, and Scandinavia. Positive anomalies are evident over Iberia and North Africa, which corroborate previous findings (Park 2004). Lastly, during October–December (OND), positive precipitation anomalies are evident over Iberia, western and southern France, northern Italy, the British Isles, and southern Scandinavia. These boreal fall anomalies over the Atlantic coastal region of southern Europe are consistent with previous findings for this region (Mariotti et al. 2002, 2005; Pozo-Vázquez et al. 2005; Shaman and Tziperman 2011).

Seasonal ENSO-based composites made using the satellite-derived precipitation estimates reveal similar patterns (not shown). Indeed, the spatial correlation of the precipitation composites made using CAMS with those made using the ECA&D data are $r = 0.75$ (JFM), $r = 0.34$ (AMJ), $r = 0.71$ (JAS), and $r = 0.79$ (OND). Clearly, the spatial correlation during the AMJ season is much weaker than in the other three seasons; however, during 1979–2011, the period of the CAMS record, there were only two AMJ La Niña events. This limited sample size likely explains the weak spatial correlation of the AMJ composites made using post-1978 satellite-derived data with those made using the longer 1950–2013 ECA&D record, for which there were 11 AMJ La Niña events.

Using the distributed precipitation composites (Fig. 1) a number of regions were defined for further analysis. The boundaries for these regions were designed to capture areas of significant precipitation modulation associated with ENSO variability. The regions are 1) The British Isles, 50°–60°N, 12°W–2°E; 2) France and the western Alps, 44°–50°N, 6°W–10°E; 3) the Baltic Sea region, 50°–64°N, 2°–30°E; and 4) Iberia, 36°–44°N, 10°W–4°E.

Raw precipitation for each of these regions was spatially averaged and compared throughout the year with coincident ENSO conditions. Figure 2 presents running 3-month seasonal correlations of Niño-3.0 with precipitation for the four regions. These correlations depict the interannual covariability of ENSO and European precipitation by season.

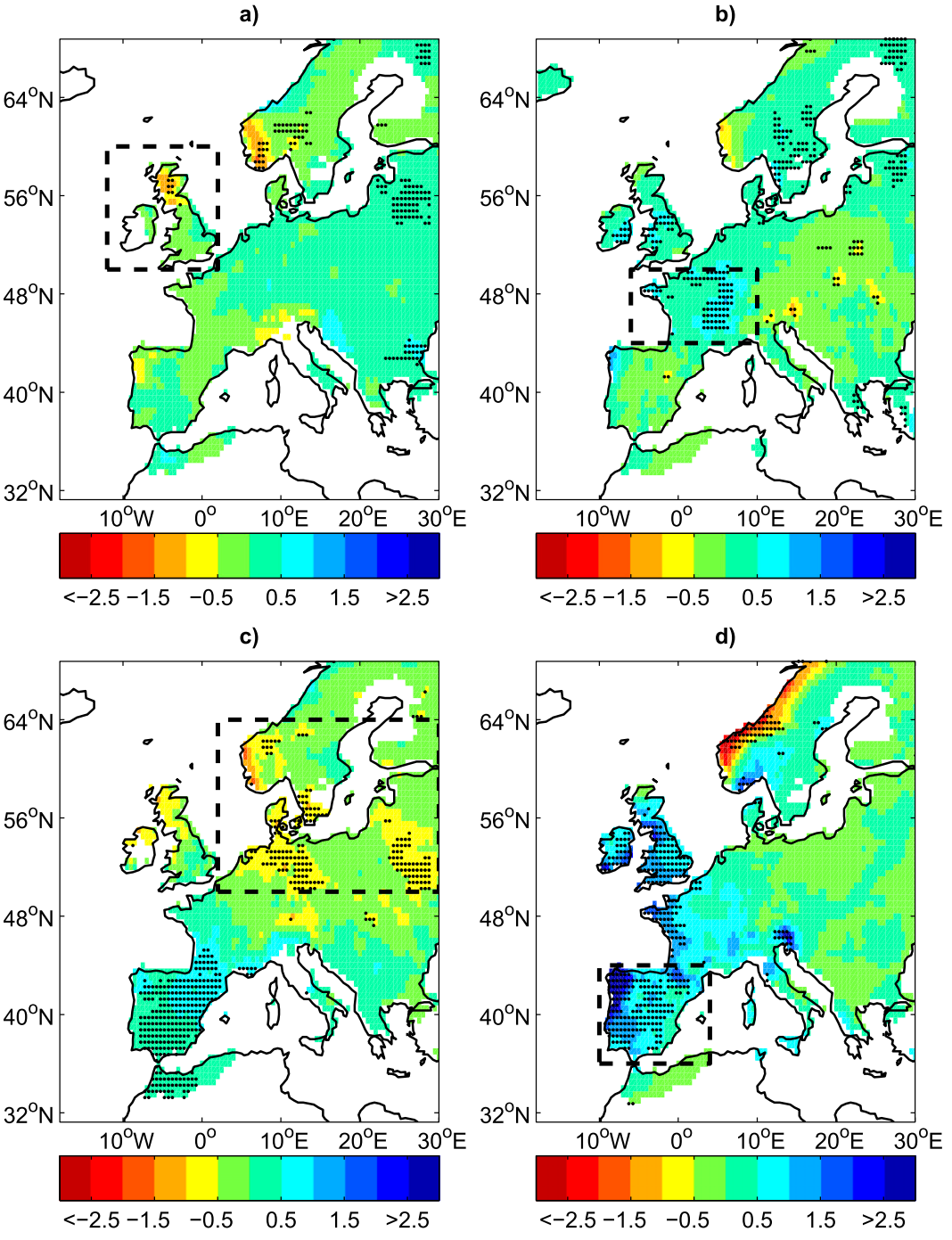

FIG. 1. 3-month seasonal ENSO-based (El Niño minus La Niña) composites of ECA&D precipitation made using Niño-3.0. Different seasons are presented in each panel: (a) JFM, (b) AMJ, (c) JAS, and (d) OND. Positive (negative) values connote increased precipitation during El Niño (La Niña) events. Units are mm day^{-1}; areas with missing data are omitted. Areas significance at the 95% level ($p < 0.05$) are dotted with black circles. Significance is based on bootstrap confidence intervals estimated through the generation of 5000 random composite maps for each 3-month period. Also shown in dashed bold are boxes outlining the four focus regions employed in this study: (a) the British Isles (50°–60°N, 12°W–2°E); (b) France and the western Alps (44°–50°N, 6°W–10°E); (c) the Baltic Sea region Europe (50°–64°N, 2°–30°E), and (d) Iberia (36°–44°N, 10°W–4°E).

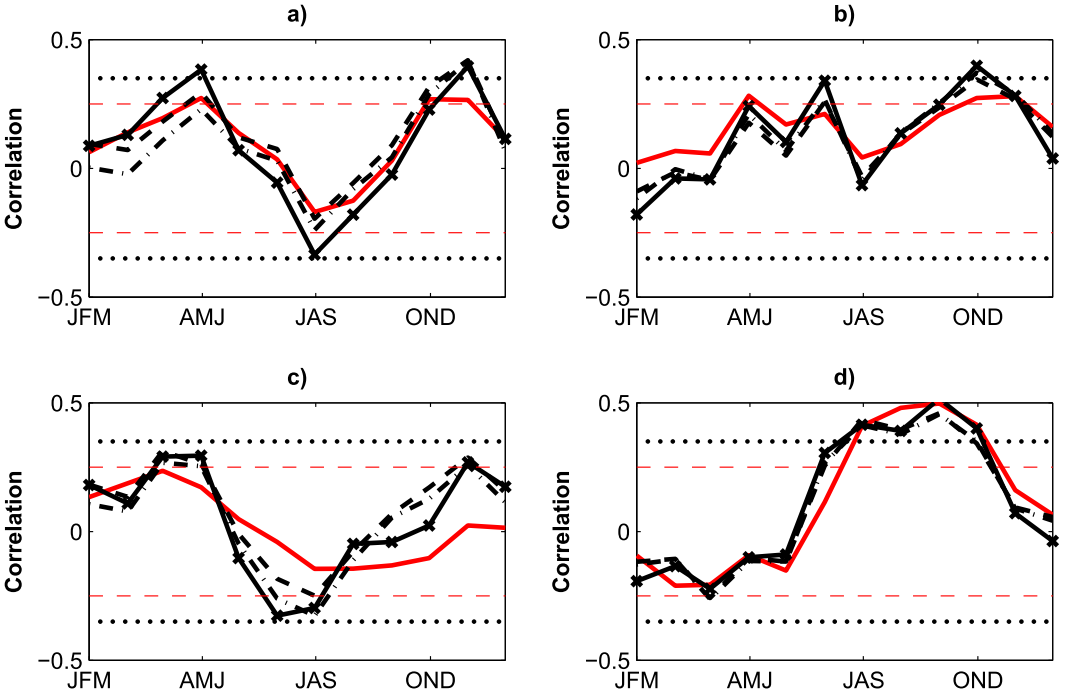

FIG. 2. Contemporaneous 3-month seasonal correlations of Niño-3.0 with precipitation in four European regions: (a) the British Isles (50°–60°N, 12°W–2°E); (b) France and the western Alps (44°–50°N, 6°W–10°E); (c) the Baltic Sea region (48°–64°N, 2°–30°E); and (d) Iberia (36°–44°N, 10°W–10°E). The solid red line is ECA&D, the solid black line is CAMS precipitation, the black dashed line is NASA precipitation, and the dashed-dotted line is CMAP precipitation. The red dashed line indicates statistical significance at $p < 0.05$ for the longer ECA&D dataset; the black dotted line indicates statistical significance at $p < 0.05$ for the other precipitation datasets.

For three of the four regions there exists a positive association with Niño-3.0 during boreal fall. More specifically, for the longer 1950–2013 ECA&D dataset, a statistically significant positive correlation with Niño-3.0 SSTs exists during AMJ, OND, and November–January (NDJ) for region 1 (British Isles) and region 2 (France and the western Alps). For the British Isles, JAS ECA&D precipitation and Niño-3.0 are negatively correlated, but not quite at the $p < 0.05$ significance level. The shorter record length satellite-derived precipitation datasets exhibit similar tendencies.

For region 3 (the Baltic Sea region) the satellite-based precipitation records and ECA&D precipitation record diverge somewhat in their seasonal correlations with ENSO. The satellite-based precipitation datasets (CAMS, CMAP, and NASA) are negatively correlated with Niño-3.0 SSTs during June–August (JJA) and JAS, albeit not at statistically significant levels. Similarly, positive correlations during the AMJ and NDJ seasons near statistical significance for the satellite-based products. The ECA&D is less correlated with Niño-3.0 throughout the year, although it approaches statistical significance during the March–May (MAM) season.

For region 4 (Iberia) seasonal correlations between Niño-3.0 SSTs and ECA&D precipitation are significant and positive for the JAS through OND seasons. Seasonal correlations of ENSO with the CAMS, CMAP, and NASA datasets are also significant and positive at this time of year.

Figure 1 shows that considerable spatial heterogeneity exists in the seasonal precipitation anomaly patterns associated with ENSO variability. However, for the three Atlantic coastal regions, running seasonal correlations indicate a tendency toward increased precipitation during fall El Niño events in the Pacific. For all but region 4 (Iberia), there is a tendency toward more precipitation during boreal spring. Over northern Europe there is reduced precipitation during boreal summer. In addition, there is little precipitation change associated with ENSO over western Europe during boreal winter.

b. Upper tropospheric response to ENSO

The effects of ENSO on upper tropospheric structure are next examined in an effort to identify ENSO-associated seasonal changes in the upper troposphere potentially associated with the presence or absence of precipitation anomalies over Europe. For brevity, only four seasons (JFM, AMJ, JAS, and OND) are presented. ENSO-based composites of JFM 200-hPa relative vorticity and zonal wind (Fig. 3) reveal a Pacific–North

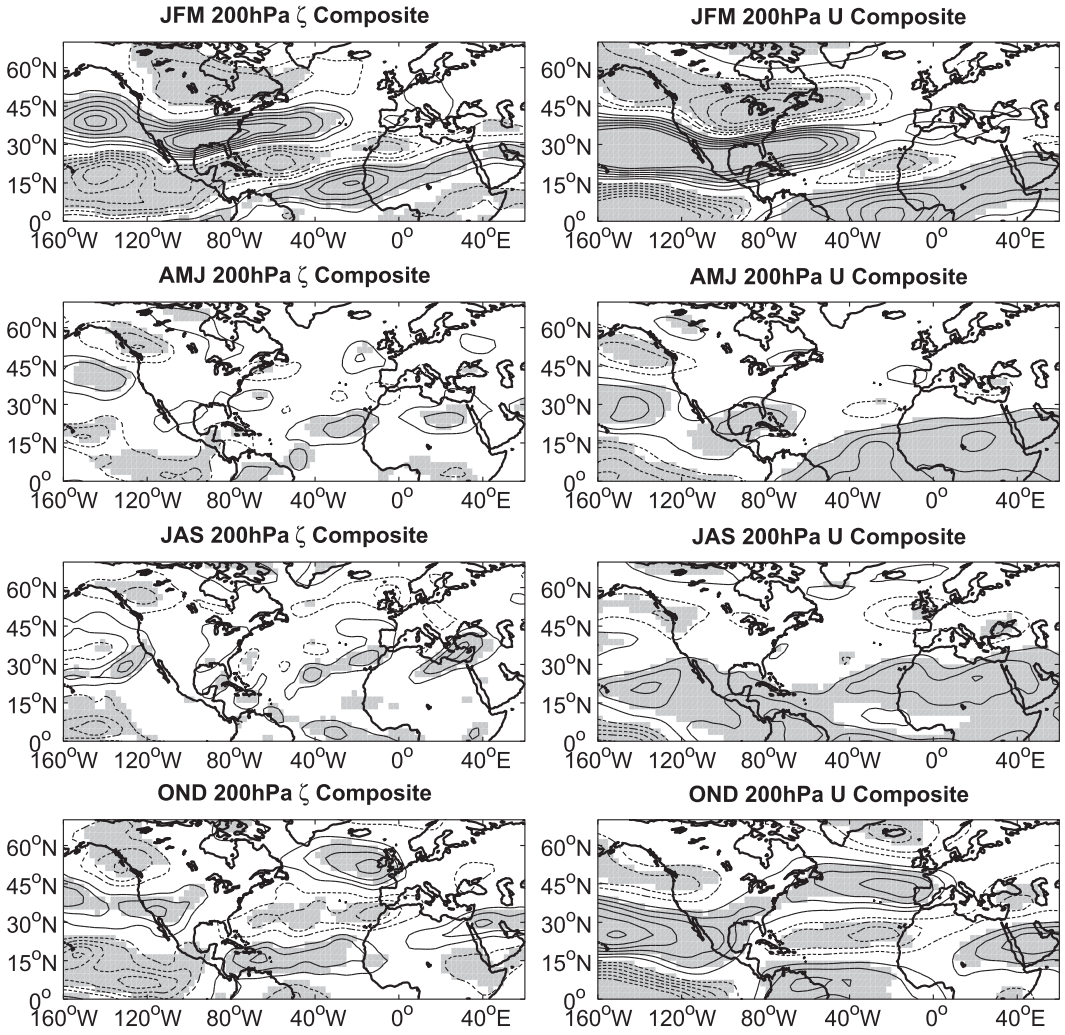

FIG. 3. 3-month seasonal ENSO-based composites of NNR 200-hPa (left) relative vorticity and (right) zonal wind made using Niño-3.0 SSTs. The contour intervals are $4 \times 10^{-6}\,s^{-1}$ (left column) and $2\,m\,s^{-1}$ (right column). Negative contours are dotted; the zero contour is omitted. Gray areas denote regions significant at the 95% level ($p < 0.05$) based on bootstrap confidence intervals estimated by generation of 5000 random composite maps for each 3-month seasonal period.

American (PNA)-like response over the North Pacific and Canada (Horel and Wallace 1981), as well as a Rossby wave train of alternately signed anomalies that has propagated from the equatorial Pacific to North America, reflected in the vicinity of the North American jet over the continental United States, and moved southeastward over the subtropical North Atlantic. This Rossby wave train and teleconnection pattern has been previously characterized and associated with changes in the North African–Asian (NAA) jet and snowfall over the Tibetan Plateau (Shaman and Tziperman 2005).

The JFM positive vorticity anomaly over the southeastern United States superimposes in latitude with the North American jet core (near 30°N). Statistically significant changes in both 200-hPa vorticity and zonal wind extend from North America to the mid-Atlantic; however, these changes fail to reach western Europe north of 40°N. Similar upper tropospheric wintertime responses have been reported previously (Dong et al. 2000), as well as analogous anomalies in mean sea level pressure fields (van Loon and Madden 1981; Fraedrich 1994). In some instances, for strong individual ENSO events (e.g., the 1997/98 El Niño), these upper tropospheric anomalies have extended eastward to western Europe (Dong et al. 2000); however, for these 1950–2013 ENSO composites, no statistically significant anomalies occur over Europe, nor is the whole field response statistically significant in the immediate North Atlantic/European sector (Table 1).

TABLE 1. Whole field statistical significance of various seasonal composites for the North Atlantic/European sector (30°–70°N, 60°W–40°E). Significance was determined per the methods of Livezey and Chen (1983) and as described in the text. Whole field composites significant at $p < 0.05$ are shown in bold.

Composite	Season			
	JFM	AMJ	JAS	OND
200-hPa relative vorticity	0.876	0.172	0.890	**0.974**
200-hPa zonal wind	0.880	0.268	0.786	**0.978**
850-hPa zonal wind	0.892	0.306	0.576	**0.960**
850-hPa meridional wind	0.726	0.624	0.686	0.942
850-hPa specific humidity	0.942	0.584	0.596	0.846
850-hPa zonal moisture flux	0.856	0.258	0.524	**0.976**
850-hPa meridional moisture flux	0.766	0.666	0.708	0.938
850-hPa $\overline{v'T'}$	0.914	0.144	0.358	0.830

During AMJ, ENSO-related variability produces little statistically significant change in the upper troposphere over the Atlantic, Europe, and North Africa, except for some changes in the NAA jet (Fig. 3). However, there is a positive vorticity anomaly to the west of France, which at its core is statistically significant. This positive anomaly forms at the end of the North Atlantic jet. Meridionally oriented dipole structures have been shown to form at jet exit regions at seasonal to interannual time scales and are indicative of zonal wind fluctuations in these areas (Blackmon et al. 1984a,b); however, these dipole structures have been more commonly noted during winter seasons [e.g., December–February (DJF)]. Still, in this instance for the AMJ season, to the south of the positive vorticity anomaly lies a weak negative vorticity anomaly at the Straits of Gibraltar. This weak AMJ dipole is similar to the stronger vorticity dipole observed in response to ENSO variability for the OND season (Mariotti et al. 2005; Shaman and Tziperman 2011); however, the AMJ dipole anomaly is statistically significant for only a limited area west of Ireland, and the North Atlantic/European whole field response is not statistically significant (Table 1).

During JAS, ENSO variability produces statistically significant changes in the NAA jet (Fig. 3), which has migrated to its most northern position. These anomalies in the NAA jet include positive vorticity anomalies west of North Africa and over the eastern Mediterranean. Positive zonal wind anomalies stretch from the subtropical Atlantic over North Africa, Arabia, and the Indian subcontinent. This boreal summer ENSO-associated variability in the NAA jet has been previously documented (Shaman and Tziperman 2007; Shaman et al. 2009). However, the whole field vorticity response is not statistically significant for the immediate North Atlantic/European region (Table 1).

To the north of the NAA jet, over the eastern Atlantic and western Europe there is a negative vorticity anomaly centered over Scotland, which extends to the west across the North Atlantic. To the northwest of this negative anomaly, a positive anomaly lies over southern Greenland, north of 65°N. These upper tropospheric vorticity anomalies are associated with positive zonal wind anomalies north of 60°N and increased flow toward Scandinavia, as well as negative, offshore zonal wind anomalies over the British Isles and France.

During the fall OND season, the ENSO-related vorticity response lies at roughly the same latitude as during the AMJ season; however, the magnitude and statistical significance of the anomalies are much greater and the positive anomaly west of France is accompanied by a large negative anomaly west of the Straits of Gibraltar (Fig. 3). As shown previously for the September–December season (Shaman and Tziperman 2011), these vorticity anomalies are associated with increased onshore flow from the Atlantic to Iberia and France. To the north and south of this increased flow negative, offshore wind anomalies are present. The whole field 200-hPa zonal wind response is statistically significant (Table 1). These OND dipole anomalies are similar in shape and position to the eastern Atlantic pattern, which has typically been defined for the DJF season (Wallace and Gutzler 1981; Blackmon et al. 1984a), or individual winter months (Barnston and Livezey 1987). The findings here indicate that this pattern of interannual variability may arise or modulate in part in response to variability in the tropical Pacific.

Over the span of a year, the upper tropospheric response to ENSO in the European sector changes substantially. During the winter, a wave train response is clear; however, the wave train anomalies are located over North America, the western Atlantic, and North Africa, indicating little change in flow patterns over northern Europe. In the other seasons, no clear stationary wave train pattern is evident, yet vorticity anomalies are present over the eastern Atlantic and western Europe. These anomalies lie to the north of the NAA jet and at the exit region of the North Atlantic jet. Indeed, model studies indicate that the atmospheric response to tropical forcing can be great in jet exit regions (Ting and Held 1990; Hoerling and Ting 1994; Held et al. 2002). This interaction with the North Atlantic jet may explain the large, somewhat isolated responses during the JAS and OND seasons over the North Atlantic, and even the weaker response evident during AMJ (Fig. 3).

Zonal winds associated with the AMJ and OND vorticity anomalies produce increased onshore flow from the Atlantic Ocean over Iberia and France. During the summer season, the vorticity dipole response is present

but weaker and appears to shift considerably northward and produces zonal wind anomalies that decrease onshore upper tropospheric flow from the Atlantic to western Europe.

Onshore wind pattern anomalies between 36° and 48°N are loosely consistent with the observed ENSO-related changes in precipitation over western and northern Europe (Figs. 1 and 2). Specifically, onshore flow increases during spring and fall at 45°N when and where precipitation is significantly positively associated with Niño-3.0 SSTs; offshore flow increases during boreal summer when and where precipitation is negatively associated with ENSO conditions. During boreal winter, no clear change emerges. As will be shown next, these changes to European precipitation in response to ENSO are linked to lower tropospheric flow patterns that manifest in association with these upper tropospheric changes.

c. *Lower tropospheric response*

The seasonal upper tropospheric changes in the North Atlantic–European sector due to ENSO appear to derive from either a Rossby wave train emanating from the equatorial Pacific (JFM) or development of a dipole anomaly structure in the exit region of the North Atlantic jet to the west of Europe (AMJ, JAS, and OND). It is next examined whether these upper tropospheric changes project to the lower troposphere and affect circulation patterns, moisture advection, or storm activity.

Figure 4 presents Niño-3.0-based composites of 850-hPa zonal wind, zonal humidity flux, and meridional humidity flux. During the JFM season, statistically significant anomalies are predominantly offshore over the Atlantic Ocean. These anomalies include easterly winds and increased humidity at the latitude of France, and southerly winds to the west of the Straits of Gibraltar. Moisture flux anomalies tend to be collocated with wind anomalies. A vector moisture flux composite (not shown) reveals anomalous cyclonic flow centered near 36°N, 55°W that contributes to the easterly moisture flux anomalies along 48°N over the North Atlantic.

The JFM 850-hPa zonal wind anomalies (Fig. 4) are located in the same positions as the 200-hPa zonal wind anomalies (Fig. 3). This superposition with height is indicative of an equivalent barotropic structure, and is consistent with the dynamics of a tropical-to-extratropical stationary barotropic Rossby wave train (Hoskins and Karoly 1981).

The lower tropospheric anomalies during the AMJ season are generally not statistically significant. The 850-hPa zonal wind anomaly structure (Fig. 4) and position matches the weak zonal wind dipole observed at 200 hPa (Fig. 3) with negative zonal wind anomalies to the west of Ireland and positive wind anomalies at the Iberian coast. The 850-hPa zonal humidity flux anomalies are similarly positioned at the European coast.

The AMJ 850-hPa meridional humidity flux anomalies are dominated by an east–west dipole along 48°N. These anomalies together with the zonal wind and humidity flux anomalies make up a cyclonic circulation centered at 48°N, 15°W. The strongest onshore fluxes of this circulation bring increased moisture onshore to northwestern France and northward over the Bay of Biscay and English Channel to the British Isles. Such flow, though weak, is consistent with increased precipitation in this region.

During the JAS season, the lower tropospheric response to ENSO is generally not statistically significant, particularly north of 40°N. Easterly (negative) zonal wind (humidity flux) anomalies are present at 850 hPa over the British Isles, and westerly (positive) zonal wind (humidity flux) anomalies lie to north over Iceland and northern Scandinavia. Although these zonal moisture flux composite anomalies are not statistically significant, given the mean westerly flow for this region (not shown), these anomalies are consistent with a reduction of onshore moisture advection to the British Isles and the Baltic Sea and the reduced precipitation observed for these regions (Figs. 1 and 2).

A statistically significant northward meridional humidity flux is evident during the JAS season over the western Mediterranean (Fig. 4). This flux brings anomalous moisture onshore to southern France and Italy, and may explain some of the increased precipitation during El Niño observed for this coastal region (Fig. 1c).

The lower tropospheric response to ENSO during the OND season is dominated by a cyclonic circulation anomaly centered to the west of Ireland that generates an anomalous westerly (positive) zonal wind (moisture flux) toward France and Iberia and an anomalous southerly (positive) meridional wind (moisture flux) over France, Britain, the North Sea, and Scandinavia (Fig. 4). This response is consistent with similar composites made for the September–November (Mariotti et al. 2005) and September–December seasons (Shaman and Tziperman 2011).

The anomalous circulation is superpositioned with the positive pole of the upper tropospheric vorticity dipole anomaly (Fig. 3). In the lower troposphere, this anomalous flow brings humid Gulf Stream air over much of western Europe as far north as Norway and is consistent with a moistening of the European continental boundary layer and increased precipitation in the region, particularly coastal, orographically induced precipitation over areas including Iberia and southern Norway. Whole field composite significance testing indicates that both the

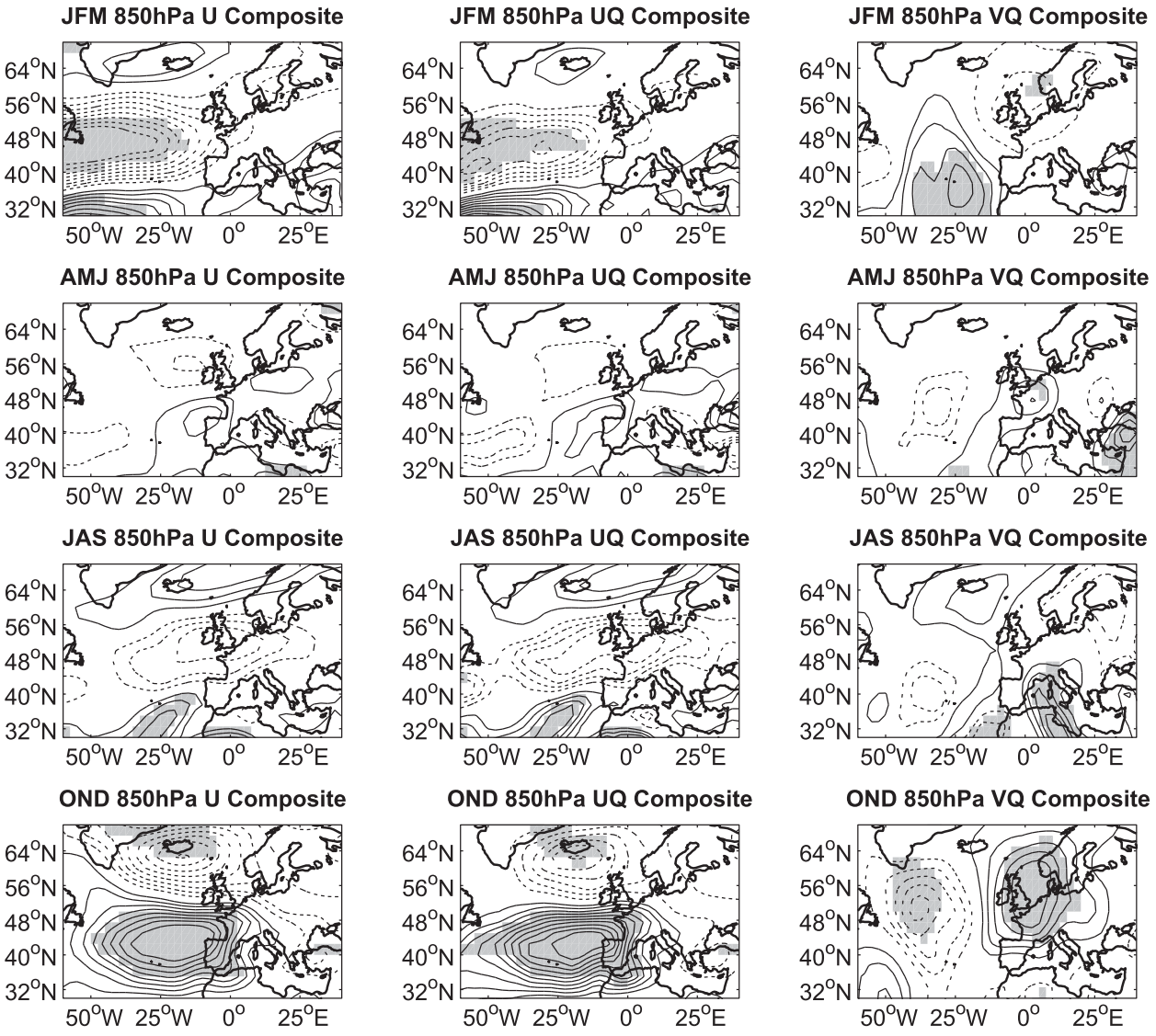

FIG. 4. 3-month seasonal ENSO-based composites of NNR (left) 850-hPa zonal wind, (middle) zonal humidity flux, and (right) meridional humidity flux made using Niño-3.0 SSTs. The contour intervals are 0.5 m s^{-1} (left column) and 1×10^{-4} (m s^{-1}) (kg kg^{-1}) (middle and right columns). Negative contours are dotted; the zero contour is omitted. Gray areas denote regions significant at the 95% level ($p < 0.05$) based on bootstrap confidence intervals estimated by generation of 5000 random composite maps for each 3-month seasonal period.

850-hPa zonal wind and zonal moisture flux composite anomalies are statistically significant (Table 1).

ENSO-associated changes in storm activity were next assessed using seasonal composite maps of 850-hPa eddy heat flux, $\overline{v'T'}$. A Butterworth filter with a half-power cutoff period of 8 days was used to high-pass filter the daily NNR record and select for variability at synoptic time scales. Individual seasonal averages were then computed from these filtered data and ENSO-based composites constructed (Fig. 5).

During the JFM season negative anomalies of 850 hPa $\overline{v'T'}$ exist at 48°N along the North Atlantic storm track, extending from the east coast of North America to the mid-Atlantic. This reduced storm activity during El Niño events, though strong, is not statistically significant; however, to the south and north significant increased storminess occurs. Positive 850-hPa $\overline{v'T'}$ anomalies cover most of Europe but are weaker than those over the North Atlantic.

During the AMJ and JAS seasons there is almost no ENSO-related change in storm activity over Europe. Over the North Atlantic, however, there are increases (decreases) of storm activity associated with El Niño during AMJ (JAS).

ENSO composite storm activity for the OND season reveals a southward shift of the North Atlantic storm

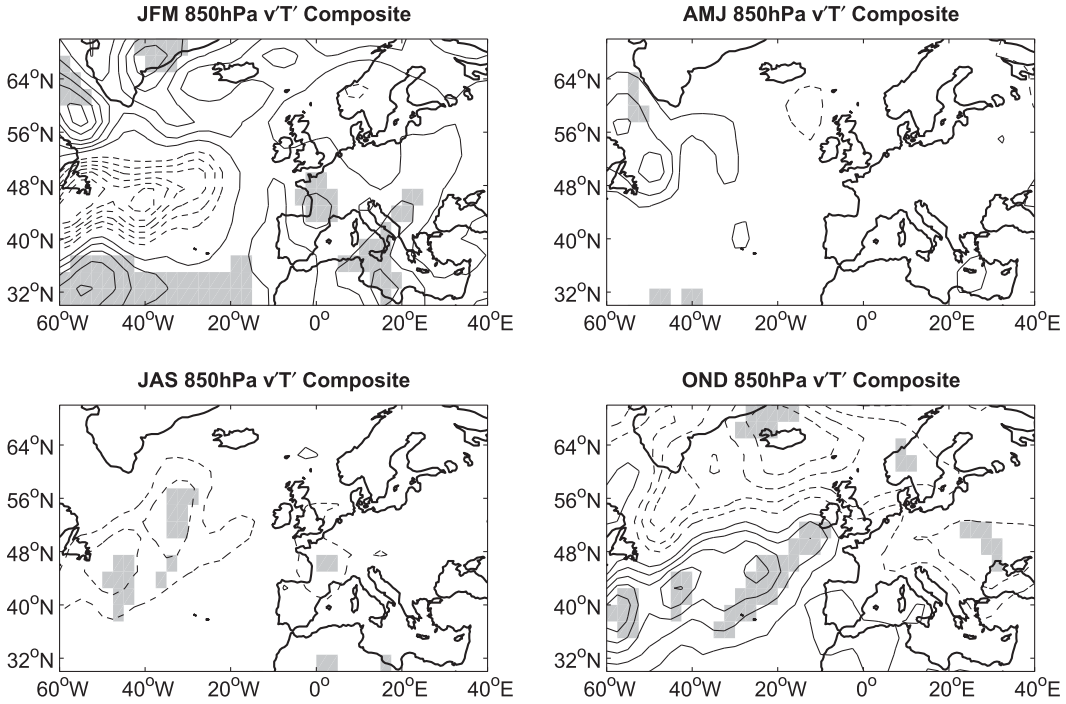

FIG. 5. 3-month seasonal ENSO-based composites of NNR 850-hPa meridional eddy heat flux ($\overline{v'T'}$) computed from high-pass filtered daily reanalysis. The contour interval is 0.5 K m s^{-1}. Negative contours are dashed; the zero contour is omitted. Gray areas denote regions significant at the 95% level ($p < 0.05$) based on bootstrap confidence intervals estimated by generation of 5000 random composite maps for each 3-month seasonal period.

track during El Niño events (Fig. 5). Statistically significant positive anomalies extend from North America to the British Isles. To the north and east of this positive anomaly, decreased synoptic activity extends over Greenland, Iceland, Scotland, Scandinavia, and central Europe.

The changes in synoptic activity associated with ENSO variability do not appear spatially coincident with ENSO-associated changes in precipitation (Fig. 1). For instance, during the OND season, precipitation increases during El Niño events over much of western Europe, as well as eastern Iceland, even though storm activity subsides over much of this region (Fig. 5). This discrepancy may stem from the incompleteness of the 850-hPa $\overline{v'T'}$ metric, which accounts for synoptic activity but does not account for other rain forms, such as drizzle from boundary layer clouds or orographically induced rainfall. Both of these rain types would potentially increase with a simple increase of the onshore flow of moist air, such as seen in Fig. 4.

4. NAO effects

The European continent lies directly downwind of the NAO and is affected by NAO-associated changes in storm activity and westerly flow. A strong association between the NAO and precipitation over Europe has been demonstrated (Hurrell and van Loon 1997; Rodó et al. 1997; Rimbu et al. 2001; Zveryaev 2004; Efthymiadis et al. 2007), and the NAO is a dominant mode of variability over the North Atlantic on decadal time scales (Hurrell 1995). Consequently, the NAO may act as a possible confounder in the present analysis. In particular, a strong correlation of ENSO and the NAO could lead to a corruption of the composite plots presented in the previous section.

To examine whether the NAO and ENSO covary, seasonal correlations between these two systems were tabulated for the 1950–2013 period (Fig. 6). For the most part these correlations fail to reach statistical significance ($p < 0.05$). For the Hurrell index, a statistically significant negative correlation is evident during late spring/early summer. For the station-based CRU index a statistically significant positive correlation with the Niño-3.4 appears during MAM. The two NAO indices themselves are most strongly correlated ($r > 0.8$) during late autumn and winter (OND through JFM) and are most weakly correlated ($r < 0.6$) during summer. Similar results are found when a shorter time period (1979–2011) is examined (not shown).

Within atmospheric general circulation model (AGCM) simulations, some studies have found evidence

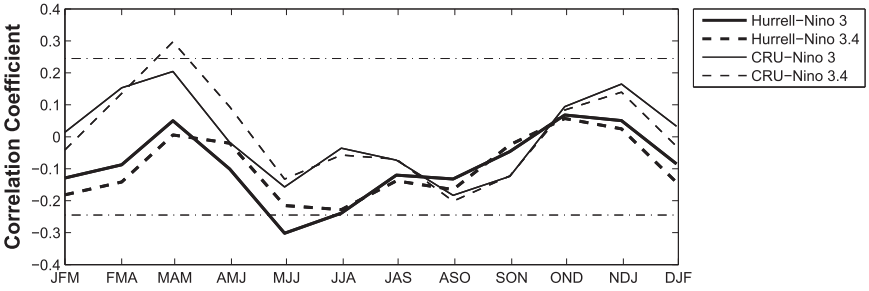

FIG. 6. Concurrent 3-month seasonal 1950–2013 correlations of the Hurrell and CRU indices for the NAO with the Niño-3.0 and Niño-3.4 indices of ENSO. The dash-dotted line indicates statistical significance at $p < 0.05$.

for a boreal winter coupling between ENSO and the NAO that varies in significance on decadal time scales (Sutton and Hodson 2003; Greatbatch and Jung 2007). In addition, Pohlmann and Latif (2005) forced an AGCM with Indo-Pacific SSTs and found that the sea level pressure response over the North Atlantic projects onto the NAO during boreal winter. Similarly, Li and Lau (2012) found that late winter NAO conditions, defined as January–February in observations, were coupled to wintertime ENSO phase during 1891–2008.

The analysis presented here finds little observational evidence of any seasonally contemporary linear coupling between the NAO and ENSO systems during the 1950–2013 study period. However, to provide a more comprehensive analysis, NAO-based composites of seasonal upper tropospheric conditions were computed and included in the MCA analysis presented in the next section.

5. Maximum covariance analysis

The analyses of precipitation (section 3a) demonstrate that associations exist between ENSO and seasonal precipitation levels over areas of Europe during several seasons. In this section, eigen techniques are used to further examine the potential role of the upper troposphere in mediating seasonal ENSO–European precipitation teleconnections. Specifically, MCA is used to identify seasonal patterns of covariability between European precipitation and upper tropospheric vorticity over the North Atlantic and Europe. The dominant patterns of covariability are then spatially correlated with ENSO- and NAO-based composites of the same fields. Correlation between the composites and MCA patterns constitutes evidence of 1) ENSO and/or NAO teleconnections to European precipitation mediated through large-scale atmospheric variability over the North Atlantic and Europe and 2) the degree to which either ENSO or the NAO seasonally impacts precipitation in the region through that atmospheric teleconnection.

MCA was performed on seasonal precipitation and 200-hPa relative vorticity fields for various regions over Europe. All fields were normalized prior to calculation of the cross-correlation matrix. The MCA findings are here presented using the region 10°–70°N, 50°W–50°E for 200-hPa relative vorticity and the region 36°–64°N, 12°W–30°E for precipitation; however, results were not sensitive to the precise domain size of either the relative vorticity or precipitation fields.

Table 2 gives the percent squared covariance for the three leading modes derived from each seasonal MCA, as well as whether those mode patterns for both precipitation and relative vorticity achieve statistically significant spatial correlation with respective composites of either ENSO or the NAO. The JFM leading mode patterns of relative vorticity and precipitation were both significantly spatially correlated with NAO composites for these fields. These findings are consistent with previous studies, which have shown that the NAO is the dominant signal in the wintertime variability of precipitation over Europe (Rimbu et al. 2001; Efthymiadis et al. 2007). This leading JFM mode (not shown) represents increased (decreased) precipitation over the northern British Isles and Scandinavia in conjunction with decreased (increased) precipitation over southern Europe during JFM, depending on the sign of the NAO.

For the AMJ season, the leading MCA mode patterns are significantly correlated with the ENSO composites

TABLE 2. Percent squared covariance for the three leading modes of each seasonal MCA of ECA&D normalized precipitation and 200-hPa NNR normalized relative vorticity. Modes for which both the precipitation and vorticity fields exhibit statistically significant ($p < 0.05$) spatial correlation with ENSO (NAO) composites are shown in bold (italics).

	Mode 1	Mode 2	Mode 3
JFM	*52.8*	29.4	1.6
AMJ	**25.7**	22.5	13.6
JAS	51.3	16.8	10.5
OND	53.8	**19.0**	*10.8*

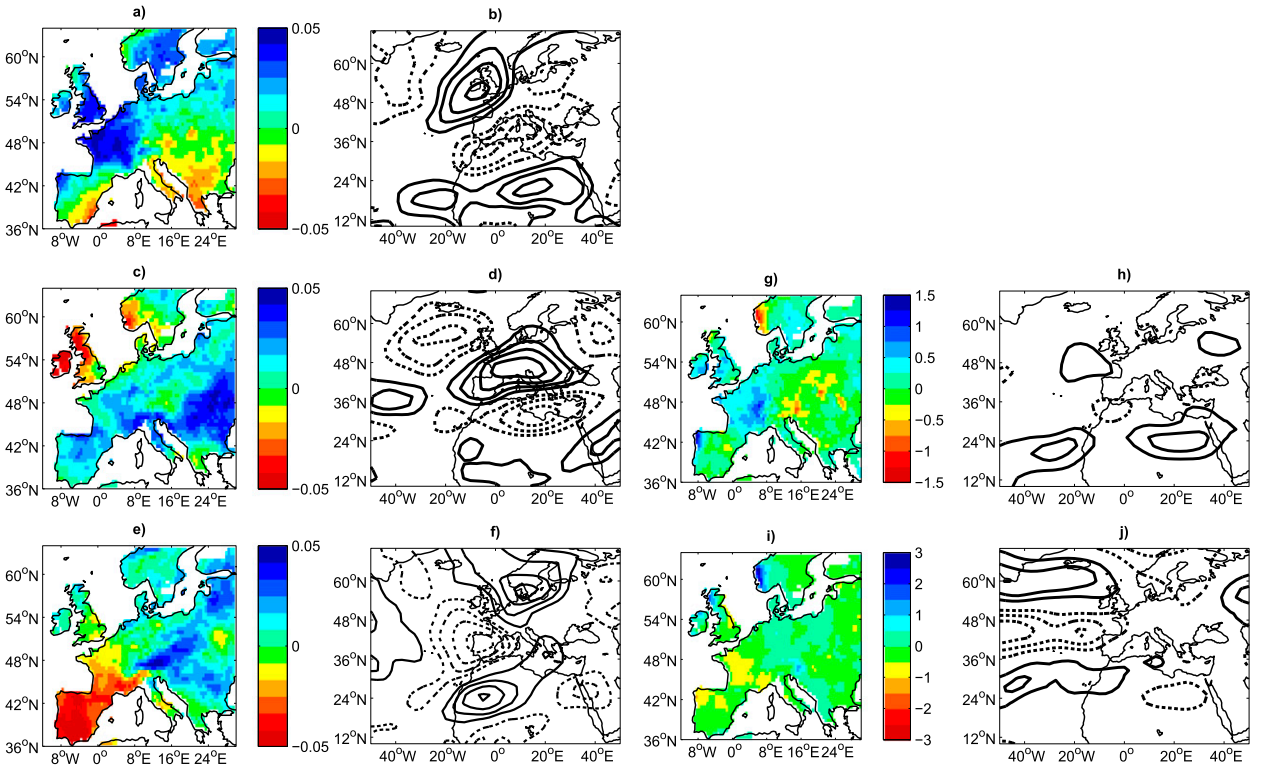

FIG. 7. MCA of AMJ ECA&D normalized precipitation and AMJ NNR normalized 200-hPa relative vorticity, as well as ENSO- and NAO-based composites of AMJ ECA&D and NNR 200-hPa relative vorticity fields. Field domains are 36°–64°N, 12°W–30°E for the precipitation and 10°–70°N, 50°W–50°E for the vorticity. The first three modes represent 25.7%, 22.5%, and 13.6% of the squared covariance for (a),(c),(e) precipitation and (b),(d),(f) relative vorticity, respectively. Also shown are ENSO composites using Niño-3.0 of (g) precipitation and (h) relative vorticity, and Hurrell NAO composites of (i) precipitation and (j) relative vorticity. Contour intervals are 0.02 in (b),(d), and (f) and $4 \times 10^{-6}\,s^{-1}$ in (h) and (j). The zero contour is omitted and dashed lines are negative.

of both precipitation and 200-hPa relative vorticity (Table 2; Fig. 7). This mode captures the increased precipitation over France, England, the Netherlands, Denmark, and Sweden, as well as the decreased precipitation along the Norwegian coast and the Mediterranean.

None of the three leading modes during the JAS season was spatially correlated with either ENSO or NAO composites at statistically significant levels. For the OND season, the second MCA mode patterns are significantly correlated with the ENSO composites and the third MCA mode patterns are significantly correlated with the NAO composites (Table 2; Fig. 8). The second mode depicts coherent changes in precipitation over Iberia, France, and England, and an opposite signed response over coastal Norway and eastern Europe. The third mode pattern for precipitation captures a north–south pattern of variability with anomalies of one sign over Great Britain and the Baltic region coincident and anomalies of the other sign over southern Europe.

Overall, portions of the seasonal covariability of European precipitation and the upper troposphere over the North Atlantic and Europe during AMJ and OND appear to represent ENSO-related variability. Specifically, leading MCA patterns match ENSO-based composites of those fields. These findings indicate that over the last 60 years ENSO has had a pronounced role in modulating the interannual variability of large-scale atmospheric conditions and precipitation in the European region during the AMJ and OND seasons.

The NAO is associated with the interannual covariability of European precipitation and the upper troposphere over the North Atlantic and Europe during the fall and winter seasons. Given that the domain used for the MCA includes much of the region used to define the NAO this pronounced linkage is not surprising. ENSO, on the other hand, is geographically remote from the domain of the MCA analysis.

6. Discussion

The analyses of observations presented here indicate that ENSO affects precipitation over western Europe throughout much of the year. This relationship varies

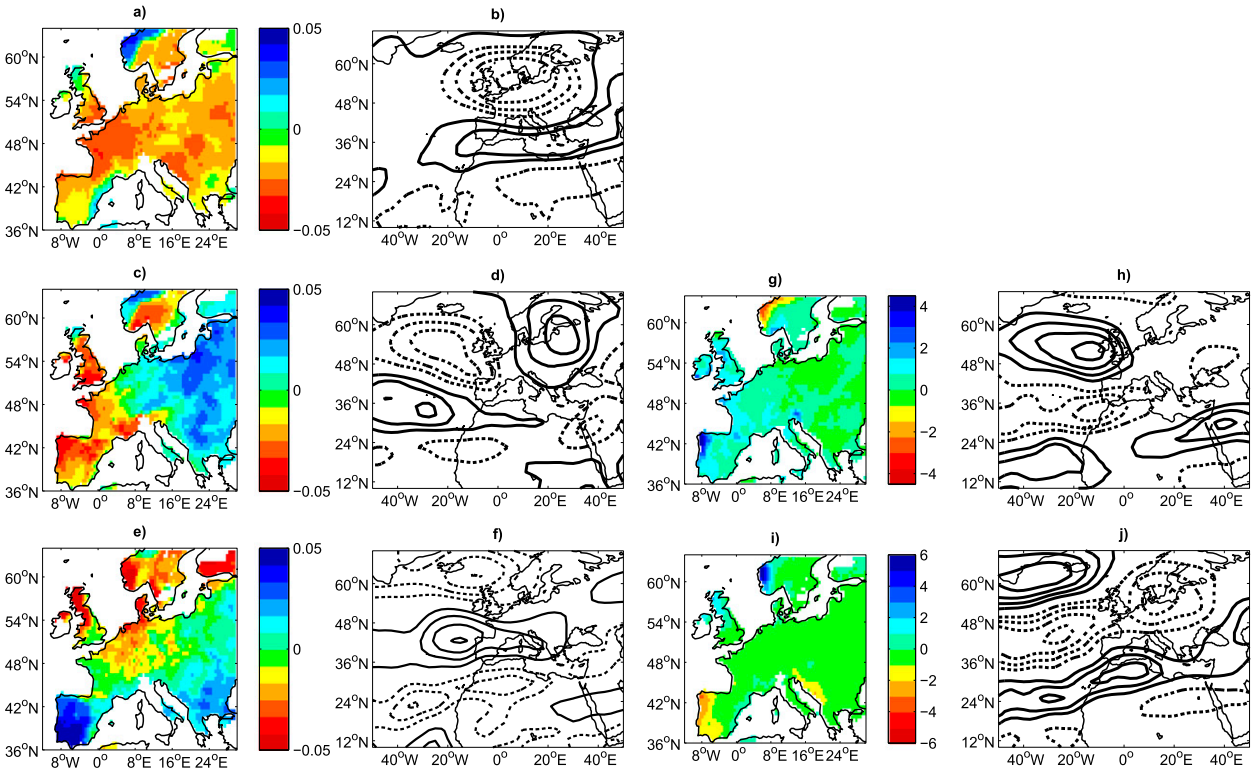

FIG. 8. As in Fig. 7, but for the OND season. The first three modes represent 53.8%, 19%, and 10.8% of the squared covariance for (a),(c),(e) precipitation and (b),(d),(f) relative vorticity, respectively. Also shown are ENSO composites using Niño-3.0 of (g) precipitation and (h) relative vorticity, and Hurrell NAO composites of (i) precipitation and (j) relative vorticity. Contour intervals as in Fig. 7.

with both the magnitude of the precipitation anomaly and the sign of the anomaly changing seasonally. The precipitation changes appear to be linked to changes in upper tropospheric conditions over the North Atlantic and Europe. In particular, during the spring and fall seasons, ENSO is associated with a dipole of vorticity anomalies in the exit region of the North Atlantic jet along the European coast. These anomalies project to the surface and alter onshore winds and moisture fluxes. A similar dipole, but of the opposite sign, manifests during boreal summer.

The seasonal upper tropospheric changes over the North Atlantic–European region appear to derive from either a clear eastward propagating Rossby wave train emanating from the equatorial Pacific (JFM) or the more isolated development of a dipole anomaly structure in the exit region of the North Atlantic jet to the west of Europe (strongly for OND, weakly for AMJ). For the OND and AMJ seasons, simulations with a simple linearized barotropic model indicate that the dipole response may also derive from an eastward propagating Rossby wave train (Shaman 2014). The source of the JAS seasonal response over the North Atlantic and Europe is less clear, although previous work indicates that ENSO excites westward propagating ultra-low-frequency Rossby waves within the NAA jet during boreal summer that reach the North Atlantic (Shaman et al. 2009). This summer season response to ENSO is also explored more fully in the companion modeling study (Shaman 2014).

Onshore moisture advection seems to be a principal driver of ENSO-related precipitation changes over western and northern Europe. Primarily, this anomalous advection stems from projections of anomalies in the upper troposphere to the lower troposphere and attendant changes in near-surface wind flow and moisture fluxes. ENSO appears to have less effect on synoptic activity over Europe during boreal spring and summer. During fall and winter, there are some ENSO-associated changes, including increased storm activity during El Niño events over southern Europe; however, while this certainly can contribute to precipitation in this region, over the examined domain (32°–70°N, 18.75°W–30°E) the pattern of the anomalous storm activity (Fig. 5) is not well correlated with ENSO-related precipitation changes (Fig. 1); for example, during the OND season the correlation coefficient between composite precipitation anomalies and composite storm activity is $r = 0.15$. Overall, the findings indicate that ENSO primarily affects precipitation over Europe through the modulation of low-level moisture advection.

From season to season the teleconnection changes considerably. A negligible precipitation response to ENSO exists on average over western Europe during boreal winter (Fig. 2). ENSO variability during JFM does produce a profound upper tropospheric response over the western and central North Atlantic (Fig. 3; see also Shaman and Tziperman 2005); however, the induced Rossby wave train passes to the west of Europe and thus does not appear to affect European precipitation. Instead, the MCA analysis indicates that European winter precipitation variability is primarily coupled with changes in the NAO (not shown), which is consistent with results from previous studies (Hurrell and van Loon 1997; Rimbu et al. 2001; Zveryaev 2004; Efthymiadis et al. 2007).

During AMJ, ENSO variability is associated with a dipole along the coast of Europe (Fig. 3) that, though relatively weak, projects to the surface producing an anomalous cyclonic circulation to the west of France (Fig. 4). This circulation brings increased moisture to northern France and Britain, and may explain the statistically significant increase in precipitation over this region (Fig. 2). The MCA analysis also indicates there is some spring season linkage to ENSO variability.

During JAS, negative precipitation anomalies over northern Europe are only tenuously associated with El Niño events in the Pacific (Fig. 1c). ENSO-based composites indicate that anomalous offshore moisture advection develops in the lower troposphere. Some linkage with ENSO-mediated changes to upper troposphere over the North Atlantic and Europe is seen in composites; however, no robust linkage is revealed through MCA analysis.

The findings here indicate that boreal fall is the season for which ENSO variability has the largest impact on precipitation conditions over the European continent. Indeed, boreal fall is the season in which, on a global basis, the greatest land area exhibits a statistically significant association between precipitation rates and ENSO phase (Mason and Goddard 2001).

The analysis also indicates that the NAO and ENSO are not well correlated; however, both phenomena, depending on the season, can affect precipitation rates over western Europe. Should these phenomena be appropriately phased, their combined influence on European weather may lead to more enhanced seasonal precipitation anomalies. However, it is not clear how the NAO and ENSO combine. Zanchettin et al. (2008) found evidence of an ENSO influence on European precipitation during winter when NAO conditions were simultaneously weak or neutral. Alternatively, Seager et al. (2010) found that the combination of an El Niño event and a negative (not weak) NAO leads to increased snowfall over northern Europe, such as happened during the winter of 2009/10. These combined effects of ENSO and the NAO need to be explored further.

A number of prior studies have found associations between ENSO and European temperature or SLP (e.g., van Loon and Madden 1981); however, only a few studies have found some association between wintertime ENSO and European precipitation, and here we found none. Efthymiadis et al. (2007) found a weak effect of ENSO on rainfall within the European Alps, which is a much smaller region than examined here. Zanchettin et al. (2008) found an association between ENSO and wintertime European precipitation when the phase of the NAO and/or PDO is factored; however, their definition of winter spanned October–March, and thus included the fall period for which there is evidence of a robust link.

Previously, boreal winter teleconnections between ENSO and European–North Atlantic near-surface fields, including sea level pressure (van Loon and Madden 1981; Greatbatch et al. 2004), temperature, and precipitation (Efthymiadis et al. 2007; Zanchettin et al. 2008), have been shown to vary on decadal time scales. This variability may be due to changes in the spatial manifestation of ENSO during a given decadal period, as the extratropical response to tropical forcing can be sensitive to the patterns of that forcing (Branstator 1985; Mathieu et al. 2004), or due to changes in downstream mean atmospheric fields, such as caused by the state of the Pacific decadal oscillation (Zanchettin et al. 2008), which may, during a particular phase, interfere with or reinforce Rossby wave propagation. In addition, volcanic activity (Brönnimann et al. 2007), stratospheric sudden warmings (Ineson and Scaife 2009), and tropical Atlantic sea surface temperatures (Park 2004) may also interact with the ENSO–North Atlantic teleconnection. The mechanisms of such interference, as well as decadal-scale variability, need to be explored further.

Future work might also examine the response of North Atlantic synoptic activity to ENSO in more detail. Analysis on these time scales might identify changes in storm activity along the North Atlantic storm track that support or intensify the observed dipole anomalies, per Fraedrich (1994). It should also be noted that the composite analysis employed here assumes that the European precipitation response to ENSO is symmetric. Evidence exists in the literature both for (Brönnimann et al. 2007) and against (in analysis of sea level pressure; Wu and Hsieh 2004) this assumption. Future analysis should be performed to examine this issue further.

The work presented here provides a baseline observational examination of the ENSO–European teleconnection throughout the calendar year. It gives evidence of the nature and seasonal variability of the atmospheric processes mediating this teleconnection. A second article

(Shaman 2014) explores the mechanisms underpinning these seasonal teleconnections in more detail.

Acknowledgments. I acknowledge the E-OBS dataset from the EU-FP6 project ENSEMBLES (http://ensembles-eu.metoffice.com) and the data providers in the ECA&D project (http://www.ecad.eu). I thank Eli Tziperman for helpful discussions. This work was supported by NSF Climate and Large-Scale Dynamics Grants AGS-1205043 and AGS-1303542.

REFERENCES

Adler, R. F., and Coauthors, 2003: The version 2 Global Precipitation Climatology Project (GPCP) monthly precipitation analysis (1979–present). *J. Hydrometeor.,* **4,** 1147–1167, doi:10.1175/1525-7541(2003)004<1147:TVGPCP>2.0.CO;2.

Barnston, A. G., and R. E. Livezey, 1987: Classification, seasonality, and persistence of low-frequency atmospheric circulation patterns. *Mon. Wea. Rev.,* **115,** 1083–1126, doi:10.1175/1520-0493(1987)115<1083:CSAPOL>2.0.CO;2.

Blackmon, M. L., Y.-H. Lee, and J. M. Wallace, 1984a: Horizontal structure of 500-mb height fluctuations with long, intermediate, and short time scales. *J. Atmos. Sci.,* **41,** 961–980, doi:10.1175/1520-0469(1984)041<0961:HSOMHF>2.0.CO;2.

——, ——, ——, and H.-H. Hsu, 1984b: Time variation of 500-mb height fluctuations with long, intermediate, and short time scales as deduced from lag-correlation statistics. *J. Atmos. Sci.,* **41,** 981–991, doi:10.1175/1520-0469(1984)041<0981:TVOMHF>2.0.CO;2.

Branstator, G., 1985: Analysis of general circulation model sea-surface temperature anomaly simulations using a linear model. Part I: Forced solutions. *J. Atmos. Sci.,* **42,** 2225–2241, doi:10.1175/1520-0469(1985)042<2225:AOGCMS>2.0.CO;2.

Bretherton, C. B., C. Smith, and J. M. Wallace, 1992: An intercomparison of methods for finding coupled patterns in climate data. *J. Climate,* **5,** 541–560, doi:10.1175/1520-0442(1992)005<0541:AIOMFF>2.0.CO;2.

Brönnimann, S., E. Xoplaki, C. Casty, A. Pauling, and J. Luterbacher, 2007: ENSO influence on Europe during the last centuries. *Climate Dyn.,* **28,** 181–197, doi:10.1007/s00382-006-0175-z.

Dong, B. W., R. T. Sutton, S. P. Jewson, A. O'Neill, and J. M. Slingo, 2000: Predictable winter climate in the North Atlantic sector during the 1997–1999 ENSO cycle. *Geophys. Res. Lett.,* **27,** 985–988, doi:10.1029/1999GL010994.

Efthymiadis, D., P. D. Jones, K. R. Briffa, R. Böhm, and M. Maugeri, 2007: Influence of large-scale atmospheric circulation on climate variability in the greater Alpine region of Europe. *J. Geophys. Res.,* **112,** D12104, doi:10.1029/2006JD008021.

Feddersen, H., 2003: Predictability of seasonal precipitation in the Nordic region. *Tellus,* **55A,** 385–400, doi:10.1034/j.1600-0870.2003.00027.x.

Fraedrich, K., 1994: An ENSO impact on Europe. *Tellus,* **46A,** 541–552, doi:10.1034/j.1600-0870.1994.00015.x.

Greatbatch, R. J., and T. Jung, 2007: Local versus tropical diabatic heating and the winter North Atlantic oscillation. *J. Climate,* **20,** 2058–2075, doi:10.1175/JCLI4125.1.

——, J. Lu, and K. A. Peterson, 2004: Nonstationary impact of ENSO on Euro-Atlantic winter climate. *Geophys. Res. Lett.,* **31,** L02208, doi:10.1029/2003GL018542.

Haylock, M. R., N. Hofstra, A. M. G. Klein Tank, E. J. Klok, P. D. Jones, and M. New, 2008: A European daily high-resolution gridded dataset of surface temperature and precipitation. *J. Geophys. Res.,* **113,** D20119, doi:10.1029/2008JD010201.

Held, I. M., M.-F. Ting, and H. L. Wang, 2002: Northern winter stationary waves: Theory and modeling. *J. Climate,* **15,** 2125–2144, doi:10.1175/1520-0442(2002)015<2125:NWSWTA>2.0.CO;2.

Hoerling, M. P., and M.-F. Ting, 1994: Organization of extratropical transients during El Niño. *J. Climate,* **7,** 745–766, doi:10.1175/1520-0442(1994)007<0745:OOETDE>2.0.CO;2.

Horel, J. D., and J. M. Wallace, 1981: Planetary-scale atmospheric phenomena associated with the Southern Oscillation. *Mon. Wea. Rev.,* **109,** 813–829, doi:10.1175/1520-0493(1981)109<0813:PSAPAW>2.0.CO;2.

Hoskins, B. J., and K. Karoly, 1981: The steady response of a spherical atmosphere to thermal and orographic forcing. *J. Atmos. Sci.,* **38,** 1179–1196, doi:10.1175/1520-0469(1981)038<1179:TSLROA>2.0.CO;2.

Hurrell, J. W., 1995: Decadal trends in the North Atlantic oscillation: Regional temperatures and precipitation. *Science,* **269,** 676–679, doi:10.1126/science.269.5224.676.

——, and H. van Loon, 1997: Decadal variations in climate associated with the North Atlantic oscillation. *Climatic Change,* **36,** 301–326, doi:10.1023/A:1005314315270.

Ineson, S., and A. Scaife, 2009: The role of the stratosphere in the European climate response to El Niño. *Nat. Geosci.,* **2,** 32–36, doi:10.1038/ngeo381.

Janowiak, J. E., and P. Xie, 1999: CAMS–OPI: A global satellite–rain gauge merged product for real-time precipitation monitoring applications. *J. Climate,* **12,** 3335–3342, doi:10.1175/1520-0442(1999)012<3335:COAGSR>2.0.CO;2.

Jones, P. D., T. Jonsson, and D. Wheeler, 1997: Extension to the North Atlantic oscillation using early instrumental pressure observations from Gibraltar and south-west Iceland. *Int. J. Climatol.,* **17,** 1433–1450, doi:10.1002/(SICI)1097-0088(19971115)17:13<1433::AID-JOC203>3.0.CO;2-P.

Kalnay, E., and Coauthors, 1996: The NCEP/NCAR 40-Year Reanalysis Project. *Bull. Amer. Meteor. Soc.,* **77,** 437–471, doi:10.1175/1520-0477(1996)077<0437:TNYRP>2.0.CO;2.

Kaplan, A., M. Cane, Y. Kushnir, A. Clement, B. Blumenthal, and B. Rajagopolan, 1998: Analyses of global sea surface temperature 1856–1991. *J. Geophys. Res.,* **103,** 18 567–18 589, doi:10.1029/97JC01736.

Kiladis, G. N., and H. F. Diaz, 1989: Global climatic anomalies associated with extremes in the Southern Oscillation. *J. Climate,* **2,** 1069–1090, doi:10.1175/1520-0442(1989)002<1069:GCAAWE>2.0.CO;2.

Knippertz, P., U. Ulbrich, F. Marques, and J. Corte-Real, 2003: Decadal changes in the link between El Niño and springtime North Atlantic Oscillation and European–North African rainfall. *Int. J. Climatol.,* **23,** 1293–1311, doi:10.1002/joc.944.

Li, Y., and N.-C. Lau, 2012: Impact of ENSO on the atmospheric variability over the North Atlantic in late winter—Role of transient eddies. *J. Climate,* **25,** 320–342, doi:10.1175/JCLI-D-11-00037.1.

Livezey, R. E., and W. Y. Chen, 1983: Statistical field significance and its determination by Monte Carlo techniques. *Mon. Wea. Rev.,* **111,** 46–59, doi:10.1175/1520-0493(1983)111<0046:SFSAID>2.0.CO;2.

Lloyd-Hughes, B., and M. A. Saunders, 2002: Seasonal prediction of European spring precipitation from El Niño–Southern Oscillation and local sea-surface temperatures. *Int. J. Climatol.,* **22,** 1–14, doi:10.1002/joc.723.

Mariotti, A., N. Zeng, and K.-M. Lau, 2002: Euro-Mediterranean rainfall and ENSO—A seasonally varying relationship. *Geophys. Res. Lett.,* **29** (12), doi:10.1029/2001GL014248.

——, J. Ballabrera-Poy, and N. Zeng, 2005: Tropical influence on Euro-Asian autumn rainfall variability. *Climate Dyn.,* **24,** 511–521, doi:10.1007/s00382-004-0498-6.

Mason, S. J., and L. Goddard, 2001: Probabilistic precipitation anomalies associated with ENSO. *Bull. Amer. Meteor. Soc.,* **82,** 619–638, doi:10.1175/1520-0477(2001)082<0619:PPAAWE>2.3.CO;2.

Mathieu, P.-P., R. T. Sutton, B. Dong, and M. Collins, 2004: Predictability of winter climate over the North Atlantic European region during ENSO events. *J. Climate,* **17,** 1953–1974, doi:10.1175/1520-0442(2004)017<1953:POWCOT>2.0.CO;2.

Moron, V., and I. Gouirand, 2003: Seasonal modulation of the El Niño–Southern Oscillation relationship with sea level pressure anomalies over the North Atlantic in October–March 1873–1996. *Int. J. Climatol.,* **23,** 143–155, doi:10.1002/joc.868.

——, and G. Plaut, 2003: The impact of El Niño–Southern Oscillation upon weather regimes over Europe and the North Atlantic during boreal winter. *Int. J. Climatol.,* **23,** 363–379, doi:10.1002/joc.890.

NCAR, cited 2013: Hurrell North Atlantic Oscillation (NAO) Index (PC-based). National Center for Atmospheric Research, Climate Analysis Section. [Available online at http://climatedataguide.ucar.edu/guidance/hurrell-north-atlantic-oscillation-nao-index-pc-based.]

Niedzielski, T., 2011: Is there any teleconnection between surface hydrology in Poland and El Niño/Southern Oscillation? *Pure Appl. Geophys.,* **168,** 871–886, doi:10.1007/s00024-010-0171-4.

Park, S., 2004: Remote ENSO influence on Mediterranean sky conditions during late summer and autumn: Evidence for a slowly evolving atmospheric bridge. *Quart. J. Roy. Meteor. Soc.,* **130,** 2409–2422, doi:10.1256/qj.03.62.

Pohlmann, H., and M. Latif, 2005: Atlantic versus Indo-Pacific influence on Atlantic–European climate. *Geophys. Res. Lett.,* **32,** L05707, doi:10.1029/2004GL021316.

Pozo-Vázquez, D., M. Esteban-Parra, F. Rodrigo, and Y. Castro-Díez, 2001: The association between ENSO and winter atmospheric circulation and temperature in the North Atlantic region. *J. Climate,* **14,** 3408–3420, doi:10.1175/1520-0442(2001)014<3408:TABEAW>2.0.CO;2.

——, S. R. Gámiz-Fortis, J. Tovar-Pescador, M. J. Esteban-Parra, and Y. Castro-Díez, 2005: El Niño–Southern Oscillation events and associated European winter precipitation anomalies. *Int. J. Climatol.,* **25,** 17–31, doi:10.1002/joc.1097.

Rimbu, N., H. Le Treut, S. Janicot, C. Boroneant, and C. Laurent, 2001: Decadal precipitation variability over Europe and its relation with surface atmospheric circulation and sea surface temperature. *Quart. J. Roy. Meteor. Soc.,* **127,** 315–329, doi:10.1002/qj.49712757204.

Rodó, X., E. Baert, and F. A. Comín, 1997: Variations in seasonal rainfall in southern Europe during present century: Relationships with the North Atlantic Oscillation and the El Niño Southern Oscillation. *Climate Dyn.,* **13,** 275–284, doi:10.1007/s003820050165.

Ropelewski, C. F., and M. S. Halpert, 1986: North American precipitation and temperature patterns associated with the El Niño/Southern Oscillation. *Mon. Wea. Rev.,* **114,** 2352–2362, doi:10.1175/1520-0493(1986)114<2352:NAPATP>2.0.CO;2.

Seager, R., Y. Kushnir, J. Nakamura, M. Ting, and N. Naik, 2010: Northern Hemisphere winter snow anomalies: ENSO, NAO and the winter of 2009/10. *Geophys. Res. Lett.,* **37,** L14703, doi:10.1029/2010GL043830.

Shaman, J., 2014: The seasonal effects of ENSO on atmospheric conditions associated with European precipitation: Model simulations of seasonal teleconnections. *J. Climate,* **27,** 1010–1028, doi:10.1175/JCLI-D-12-00734.1.

——, and E. Tziperman, 2005: The effect of ENSO on Tibetan Plateau snow depth: A stationary wave teleconnection mechanism and implications for the South Asian monsoons. *J. Climate,* **18,** 2067–2079, doi:10.1175/JCLI3391.1.

——, and ——, 2007: The summertime ENSO–North African–Asian jet teleconnection and implications for the Indian monsoons. *Geophys. Res. Lett.,* **34,** L11702, doi:10.1029/2006GL029143.

——, and ——, 2011: An atmospheric teleconnection linking ENSO and southwestern European precipitation. *J. Climate,* **24,** 124–139, doi:10.1175/2010JCLI3590.1.

——, S. K. Esbensen, and E. D. Maloney, 2009: The dynamics of the ENSO–Atlantic hurricane teleconnection: ENSO-related changes to the North African–Asian jet affect Atlantic basin tropical cyclogenesis. *J. Climate,* **22,** 2458–2482, doi:10.1175/2008JCLI2360.1.

Sutton, R. T., and D. L. R. Hodson, 2003: Influence of the ocean on North Atlantic climate variability 1871–1999. *J. Climate,* **16,** 3296–3313, doi:10.1175/1520-0442(2003)016<3296:IOTOON>2.0.CO;2.

Ting, M.-F., and I. M. Held, 1990: The stationary wave response to a tropical SST anomaly in an idealized GCM. *J. Atmos. Sci.,* **47,** 2546–2566, doi:10.1175/1520-0469(1990)047<2546:TSWRTA>2.0.CO;2.

van Loon, H., and R. A. Madden, 1981: The Southern Oscillation. Part I: Global associations with pressure and temperature in northern winter. *Mon. Wea. Rev.,* **109,** 1150–1162, doi:10.1175/1520-0493(1981)109<1150:TSOPIG>2.0.CO;2.

Vicente-Serrano, S. M., 2005: El Niño and La Niña influence on droughts at different timescales in the Iberian Peninsula. *Water Resour. Res.,* **41,** W12415, doi:10.1029/2004WR003908.

Von Storch, H., and F. W. Zwiers, 2001: *Statistical Analysis in Climate Research.* Cambridge University Press, 484 pp.

Wallace, J. M., and D. S. Gutzler, 1981: Teleconnections in the geopotential height field during the Northern Hemisphere winter. *Mon. Wea. Rev.,* **109,** 784–811, doi:10.1175/1520-0493(1981)109<0784:TITGHF>2.0.CO;2.

Wu, A., and W. W. Hsieh, 2004: The nonlinear association between ENSO and the Euro-Atlantic winter sea level pressure. *Climate Dyn.,* **23,** 859–868, doi:10.1007/s00382-004-0470-5.

Xie, P. P., and P. A. Arkin, 1997: Global precipitation: A 17-year monthly analysis based on gauge observations, satellite estimates, and numerical model outputs. *Bull. Amer. Meteor. Soc.,* **78,** 2539–2558, doi:10.1175/1520-0477(1997)078<2539:GPAYMA>2.0.CO;2.

Zanchettin, D., S. W. Franks, P. Traverso, and M. Tomasino, 2008: On ENSO impacts on European wintertime rainfalls and their modulation by the NAO and the Pacific multi-decadal variability described through the PDO index. *Int. J. Climatol.,* **28,** 995–1006, doi:10.1002/joc.1601.

Zveryaev, I., 2004: Seasonality in precipitation variability over Europe. *J. Geophys. Res.,* **109,** D05103, doi:10.1029/2003JD003668.